Journal of Applied Electrochemistry **32**: 25–34, 2002.

Mass transfer ambiguities in swirling pipe flows

S. MARTEMIANOV[1]* and V.L. OKULOV[1,2]
[1]*Laboratoire d'Etudes Thermiques UMR CNRS no. 6608, ESIP, 40, Avenue du Recteur Pineau, 68022 Poitiers Cedex, France*
[2]*Institute of Thermophysics, Lavrentyev Ave. 1, 630090, Novosibirsk, Russia*
*(*author for correspondence, e-mail: martemianov@esip.univ-poitiers.fr)*

Received 13 March 2001; accepted in revised form 18 October 2001

Key words: helical symmetry, mass transfer, mathematical model, swirl flows, vortex

Abstract

A mathematical model of mass transfer in the boundary layer of swirl flow is developed. The equations obtained for Sherwood number and mass transfer coefficient generalize the equations obtained by Levich for the flat plate to the case of mass transfer in axisymmetrical swirl flow. For the first time it is shown that, in swirl flows, the mass transfer is not completely controlled by integral flow parameters (Reynolds number and the swirl number) but depends essentially on the type of vortex symmetry. The left-handed helical vortices generate wake-like swirl flows and increase mass transfer in comparison with axial flows. The right-handed helical vortices generate jet-like swirl flows, which can decrease mass transfer.

List of symbols

c	concentration of species (mol m^{-3})
d_h	hydraulic diameter (m)
D	molecular diffusivity ($m^2\ s^{-1}$)
E	axial flux of energy (kg $m^2\ s^{-1}$), dimensionless parameter: $E/\rho U^3 R^2$
G	flow circulation ($m^2\ s^{-1}$), dimensionless parameter: G/RU
J	axial flux of momentum (kg $m\ s^{-1}$), dimensionless parameter: $J/\rho U^2 R^2$
k	mass transfer coefficient on the wall (m s^{-1})
$2\pi l$	pitch of vortex lines (m), dimensionless parameter: l/R
L	length of a cylindrical mass transfer section (m)
M	axial flux of angular momentum (kg $m^2\ s^{-2}$), dimensionless parameter: $M/\rho U^2 R^3$
n	empirical power factor
p	pressure (kg $m\ s^{-2}$), dimensionless parameter: $p/\rho U^2$
p_0	static pressure in the system (kg $m\ s^{-2}$), dimensionless parameter: $p_0/\rho U^2$
$R = d_h/2$	radius of a cylindrical mass transfer section (m)
Re	Reynolds number
Q	volumetric flow rate (kg s^{-1}), dimensionless parameter: $Q/\rho U R^2$
Sc	Schmidt number
S	swirl number
S_d	design swirl number
Sh	Sherwood number
$U = Q/\Sigma$	mean axial velocity (m s^{-1})
$V \equiv w_\varphi\ (R)$	tangential velocity of inviscid flow on a wall (m s^{-1})
w_0	velocity on a flow axis (m s^{-1}), dimensionless parameter: w_0/U
$W \equiv w_z(R)$	axial velocity of inviscid flow on a wall (m s^{-1})
(r, φ, z)	cylindrical coordinate system in inviscid flow (m, rad, m)
z	coordinate oriented along the flow (m)
$(0, w_\varphi, w_z)$	velocity components of inviscid flow (m s^{-1})
$(u_x = u_\varphi;\ u_y = -u_r;\ u_z)$	velocity components in boundary layer (m s^{-1})
(x, y, z)	coordinate system in boundary layer (m)
$y = R - r$	distance from the wall in the normal direction (m)
x	coordinate in the tangential direction (m)
Greek letters	
α	empirical constant

Γ	vortex circulation ($m^2\,s^{-1}$), dimensionless parameters: Γ/RU
δ	diffusion boundary layer thickness (m)
ε	radius of vortex core (m), dimensionless parameter: ε/R
μ	dynamic viscosity of a fluid ($kg\,m^{-1}\,s^{-1}$)
ν	kinematic viscosity of a fluid ($m^2\,s^{-1}$)
ρ	fluid density ($kg\,m^{-3}$)
τ_φ, τ_z	local shear stress at the tube wall ($kg\,m^{-1}\,s^{-2}$)
ω_z	axial component of a vorticity (s^{-1})
ω_φ	tangential component of a vorticity (s^{-1})

1. Introduction

Swirl flows have a wide range of applications in various engineering areas. Experimental data [1–9] reveal a different influence of swirl on mass transfer in annular and cylindrical tubes. Swirl usually increases mass transfer, but there are several regimes where the mass transfer coefficient is smaller in a swirl flow than in an axial flow [2, 3, 5]. From the hydrodynamic point of view the major reason for this duality lies in the incomplete understanding of possible types of swirl flow. According to the traditional approach [1–8] all swirl flows (laminar and turbulent, steady and unsteady, two dimensional and three dimensional) can be classified into two different types: (i) continuous swirl flows which maintain their characteristics over the entire length of mass transfer section; and (ii) decaying swirl flows. This classification is not complete, as it does not take into account a very important feature of swirl flows: the existence of vortex structures with different symmetry, right or left-handed helical vortices [10]. Recent progress in the study of these vortex structures reveals the direct relation between the type of vortex symmetry and the appearance of swirl flows with jet-like or wake-like profile of the axial velocity [11–13]. Both of these types of swirl flows can be continuous or decaying. Further studies [14–17] have shown that, under the same integral flow parameters (flow rate, flow circulation, axial fluxes of momentum, angular momentum and energy) both left-handed and right handed vortex symmetry can be obtained, and there is even a possibility of transition from one to another type of symmetry in the same flow. For this reason, the study of the influence of vortex symmetry on mass transfer in swirl flows is of a great interest. This aspect of a mass transfer problem in swirl flow has not previously been studied. This is the first attempt to model the mass transfer in swirl flows with different helical symmetry of the vorticity field.

2. Flow parameters and model approximations

Reynolds and Schmidt numbers are used for identification of convective mass transfer:

$$Re = \frac{U d_h}{\nu} \tag{1a}$$

$$Sc = \frac{\nu}{D} \tag{1b}$$

In swirl flows an additional parameter, the swirl number, must be taken into consideration. The definition of the swirl number varies from author to author. One of the most general forms of definition of the swirl number in a cylindrical tube of radius R was proposed [13] as:

$$S = \frac{\int_0^R w_\varphi w_z r^2\,\mathrm{d}r}{R\int_0^R w_z^2 r\,\mathrm{d}r} \tag{2}$$

Here w_φ and w_z are tangential and axial components of the mean flow velocity, r is radial coordinate.

In practical studies and engineering applications, the swirl number is replaced by a simpler parameter, the 'design swirl number'. Usually the design swirl number depends only on the geometrical parameters of the swirl generator or on the geometry of the vortex device. For example, in [1, 2] the ratio between the tangential inlet diameter and the annular channel gap was introduced as the swirl number, instead of Equation 2. In [4–7] the swirl number was defined as the angle between swirler vane and duct axis. The design swirl number definitely correlates with the more general Equation 2, but this correlation is specific for each installation.

Usually [5] the hydrodynamics and the mass transfer data in swirl flows are correlated by means of the equation

$$Sh = \alpha Re^n Sc^{1/3} \tag{3}$$

where Sh is the Sherwood number, and the empirical constant α and the power n are determined as functions of geometrical parameters of swirl generator or vortex set-up. In other words, Equation 3 postulates that only three parameters, namely Reynolds (Re), Schmidt (Sc) and swirl (S) numbers govern mass transfer in swirl flows.

In reality, the Reynolds and swirl numbers do not determine only one regime in swirl flow. For example, four different flow regimes were observed in [10] in the same set-up for identical Reynolds and swirl numbers. The reason for these ambiguities is related to different types of vortex symmetry. Ambiguities in flow regimes lead to mass transfer ambiguities. This means that traditional parameters (Equations 1 and 2) are, in general, insufficient for the prediction of mass transfer

in swirl flows. Here we propose a new approach for the prediction of mass transport in swirl flows. The above mentioned ambiguities in flow regimes will be taken into account by means of recently developed theory of helical vortex structures [10]. The equations for Sherwood number will be obtained by means of classical methodology for hydrodynamical and diffusion boundary layers at high Reynolds and Schmidt numbers.

To simplify the mathematical calculations we shall consider the simplest case of a swirl flow in a cylindrical mass transfer section of radius R and length L. Some additional assumptions are made:

(i) flow regime is steady and axisymmetric; the influence of turbulent pulsations and three-dimensional effects are neglected
(ii) the mass transfer section is short, so the developing hydrodynamic boundary layer does not essentially influence the inviscid flow core
(iii) the mass transfer does not influence the hydrodynamics
(iv) the Schmidt number is large ($Sc > 1000$), so the diffusion layer is contained within the hydrodynamic boundary layer
(v) the curvature of hydrodynamic and diffusion boundary layers is small in comparison with the tube radius
(vi) the concentration of species at the wall of the mass transfer section is constant (zero for fast electrochemical reactions) and differs from the concentration in the flow core
(vii) for electrochemical processes the effect of migration is neglected (excess of supporting electrolyte).

We use all these simplifications in our model to achieve two main goals: (a) to demonstrate that for swirl flows it is possible to calculate the Sherwood number as a function of parameters of the inviscid flow core (in the same way as by Levich for the flat plate [18]); and (b) to demonstrate the influence of the type of vortex symmetry on mass transfer.

3. A hydrodynamic model of an inviscid flow

Here we consider swirl flows induced by axisymmetric helical vortices. Let us suppose that the vortex axis coincides with the axis of the cylindrical mass transfer section and that the vortex core has radius $\varepsilon < R$ (Figure 1). We assume that the vortex core consists of helical vortex lines of a constant pitch, $2\pi l$, and has a constant axial component of vorticity:

$$\frac{\omega_\varphi}{\omega_z} = \frac{r}{l} \quad \text{and} \quad \omega_z = \frac{2\Gamma}{\varepsilon^2}\begin{cases} 1, & r < \varepsilon \\ 0, & r \geq \varepsilon \end{cases} \tag{4}$$

The spatial step-shape distribution of vorticity Equation 4 is equivalent to a Rankine vortex when l is equal to infinity [10].

The inviscid velocity field, which corresponds to the vorticity distribution Equation 4, has the next form:

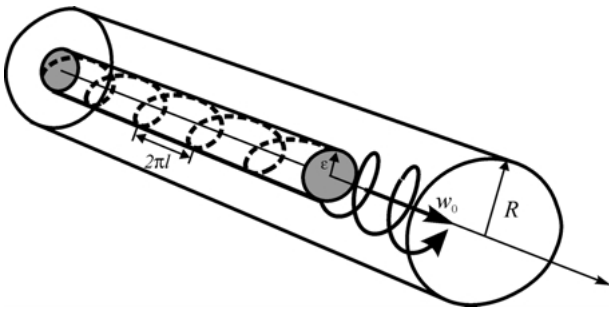

Fig. 1. Axisymmetric helical vortex structure generating a swirl flow in a tube. Key: (*dashed line*) shape of helical vortex lines which form the vortex core; ε – radius of the core; (*solid line*) trajectory of motion of fluid particles.

$$w_\varphi = \frac{\Gamma}{r}\begin{cases} r^2/\varepsilon^2, & r < \varepsilon \\ 1, & r \geq \varepsilon \end{cases} \quad \text{and}$$
$$w_z = w_0 - \frac{\Gamma}{l}\begin{cases} r^2/\varepsilon^2, & r < \varepsilon \\ 1, & r \geq \varepsilon \end{cases} \tag{5}$$

Here Γ is a vortex circulation; w_0 is the velocity on the flow axis (Figure 1). On the one hand, the velocity field Equation 5 is the exact solution of the Euler equations [19]. On the other hand, Equation 5 gives a good approximation of experimental data for various swirl flows [10, 14–17]. The comparison between Equation 5 and experimental data of [20–22] (set-ups with different swirlers) is presented on Figures 2–4. Equation 5 may be used for modeling the inviscid flow for significant distances along the tube axis. This fact is demonstrated by Figure 3 where correlation of experimental data with Equation 5 is given for velocity profiles measured at two cross-sections located at a distance of eight tube radii from each other.

A swirl flow may be described by a set of integral flow parameters. We do not take into account the influence of friction losses on the inviscid flow core. This leads to conservation laws for five integral parameters of inviscid axisymmetric flow [15]:

$$Q = 2\pi\rho \int_0^R w_z r \, \mathrm{d}r \text{ (flow rate)} \tag{6a}$$

$$G = 2\pi R w_\varphi(R) \text{ (velocity circulation)} \tag{6b}$$

$$M = 2\pi\rho \int_0^R w_\varphi w_z r^2 \mathrm{d}r \text{ (axial flux of angular momentum)} \tag{6c}$$

$$J = 2\pi\rho \int_0^R \left(w_z^2 + \left(\int_0^r \frac{w_\varphi^2}{\sigma} \mathrm{d}\sigma + \frac{p_0}{\rho} \right) \right) r \, \mathrm{d}r$$
(axial flux of momentum) (6d)

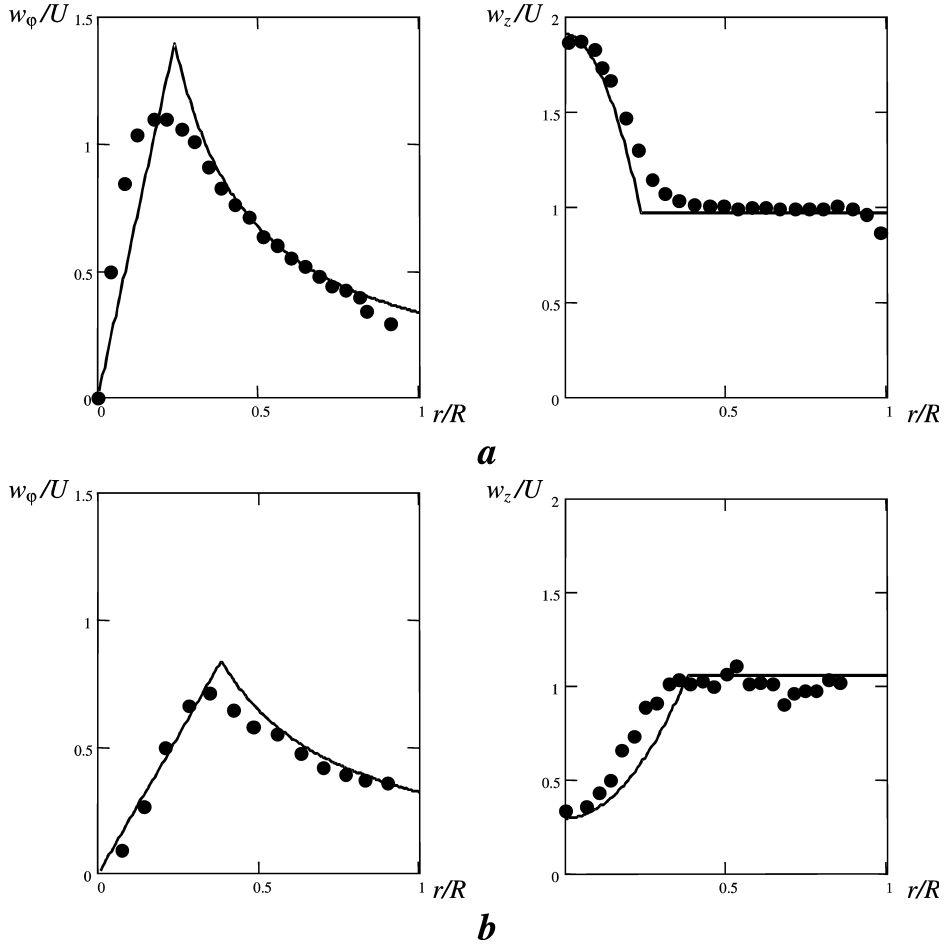

Fig. 2. Swirl flow with vortex breakdown generated by tangential vane swirler [20]. Velocity profiles before (a) and after (b) breakdown: (*points*) measured velocity profiles; (*solid lines*) approximations by Equation 5.

$$E = 2\pi\rho \int_0^R \left(\frac{w_z^2 + w_\varphi^2}{2} + \left(\int_0^r \frac{w_\varphi^2}{\sigma} \mathrm{d}\sigma + \frac{p_0}{\rho} \right) \right) w_z r \, \mathrm{d}r$$

(axial flux of energy) (6e)

Here ρ is fluid density and p_0 is a static pressure in the system.

Let us study the vortex structures (Equation 5) which may exist in the flow for given values of integral parameters (Equation 6). After substituting the velocity profile (Equation 5) in Equations 6(a)–(e), we obtain an equation which defines the vortex parameters Γ, l, ε, w_0, p_0. This system leads to the nonlinear equation for the radius of the vortex core ε [14–16]. The dimensionless form of this equation is

$$w_0(\varepsilon)\left(-\frac{w_0(\varepsilon)}{2} Q + J + \frac{\pi}{2}\frac{G^2}{l(\varepsilon)^2}\left(1 - \frac{2}{3}\varepsilon^2\right) + \pi G^2\left(\frac{1}{4} - \ln\varepsilon\right)\right) + \pi\frac{G}{l(\varepsilon)}\left(p_0(\varepsilon)\left(1 - \frac{\varepsilon^2}{2}\right) + \frac{G^2}{2l(\varepsilon)^2}\left(1 - \frac{3}{4}\varepsilon^2\right) + G^2\left(\frac{1}{\varepsilon^2} - \frac{2}{3}\right)\right) = E \qquad (7)$$

Investigation of Equation 7 for some given values of flow integrals, Γ, Q, M, J and E indicates the existence of two values for the parameter ε ($0 \le \varepsilon \le R$) [14–17]. The first root ε_1 corresponds to a positive value of l in Equations 4 and 5 and to a jet-like swirl flows, when the axial velocity has a maximum on the flow axis (Figure 5(a)). We call these types of vortex structure ($l > 0$) right-handed helical vortices. The second root ε_2 corresponds to a negative value of l in Equations 4 and 5 and to a wake-like swirl flow, when the axial velocity has a minimum on the flow axis (Figure 5(b)). We call these types of vortex structure ($l < 0$) left-handed helical vortices.

So, under the same integral parameters Equation 6, two different vortex structures may exist in swirl flow. Moreover, the transition from one vortex structure to another is also possible within the same flow regime in a cylindrical tube, for example, in flows with vortex breakdown. Concrete illustration of the existence the right and the left handed vortex structures was obtained by means of experimental data [20], see Figure 2 and Table 1. In this case the first root ε_1 corresponds to the jet-like swirl flow before the breakdown and the second one (ε_2) corresponds to the wake-like flow after the breakdown (Table 1).

Another example of the existence of two vortex structures with different helical symmetry is shown on

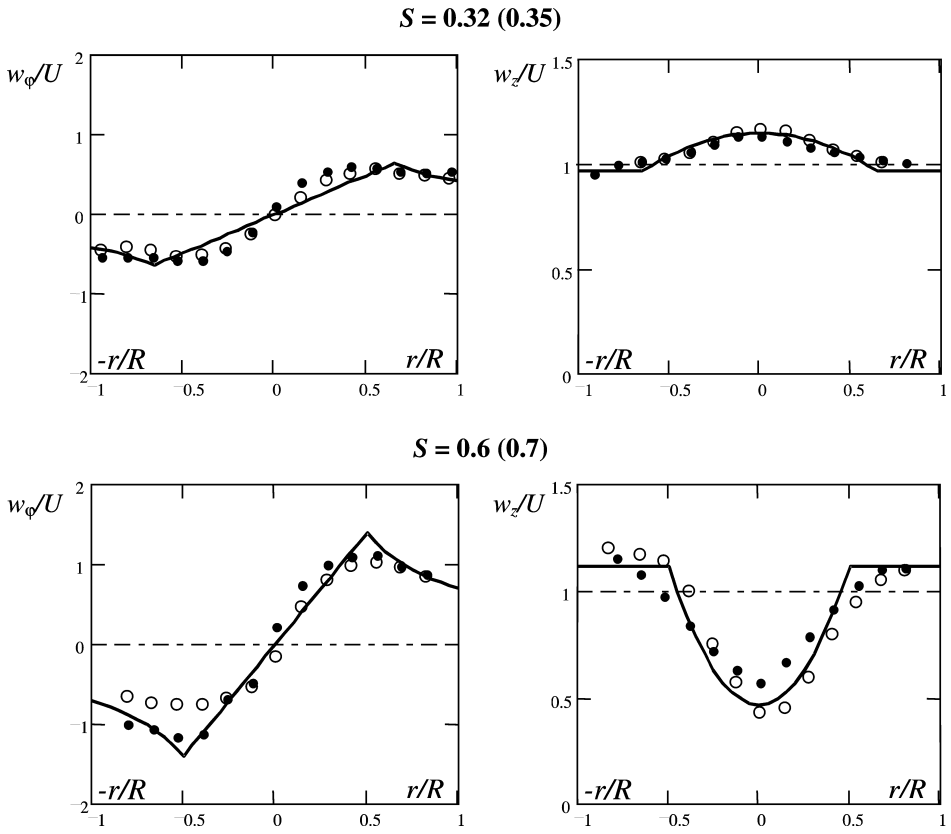

Fig. 3. Swirl flows in a tube generated by axial-tangential inlet [21]. Flows with the same flow rate ($Re = 2.8 \times 10^5$) and different swirl numbers (S): (*points*) velocity profiles measured in [21] in the first cross-section; (*circles*) velocity profiles measured in [21] in the second cross-section; (*solid lines*) approximations by Equation 5.

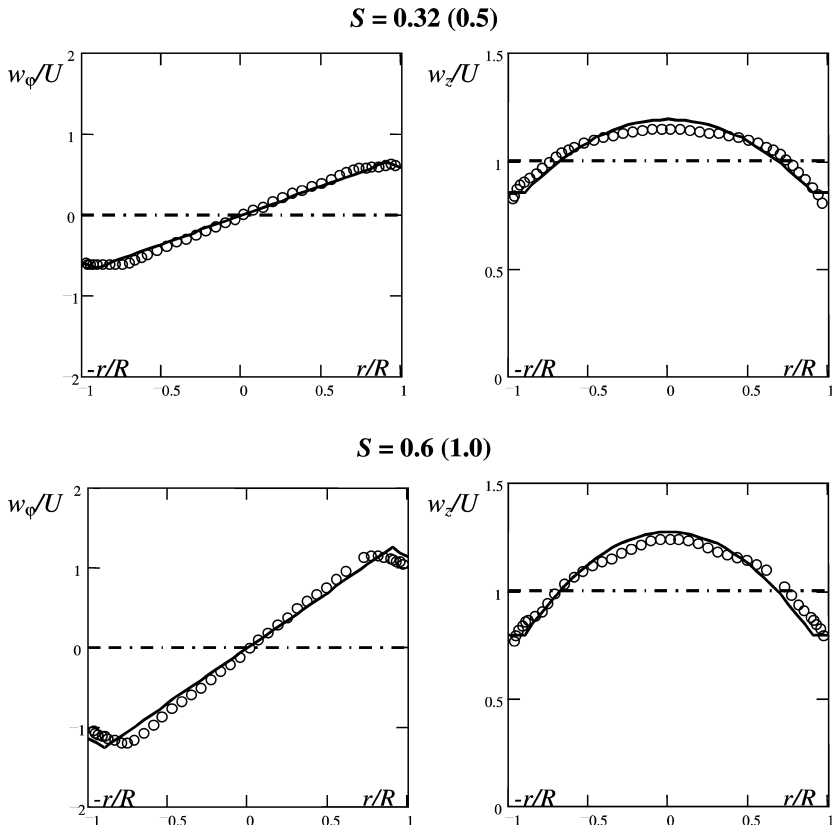

Fig. 4. Swirl flows in a tube generated by rotation of honeycomb section [22]. Flows with the same flow rate ($Re = 2.8 \times 10^5$) and different swirl numbers (S): (*circles*) velocity profiles measured in [22]; (*solid lines*) approximations by Equation 5.

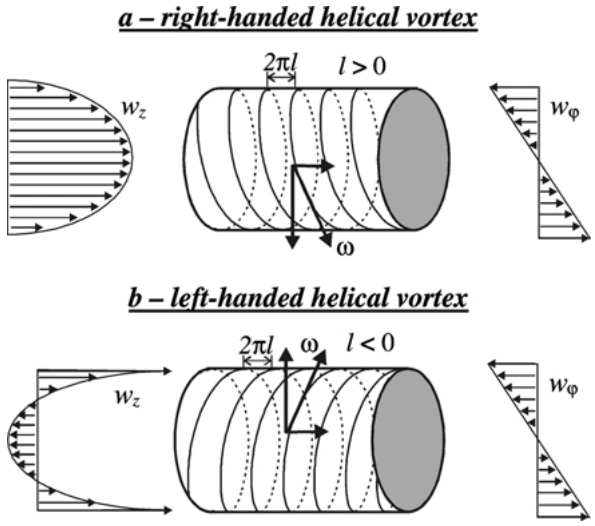

Fig. 5. Profiles of axial (w_z) and tangential (w_φ) velocities in swirl flows with right (a) and left-handed (b) symmetry of helical vortexes.

Figure 6. These two different velocity profiles were obtained under the same integral flow parameters (Table 1) by means of numerical simulation. In this case, both vortex structures have identical values of the tangential velocity near the tube wall, but the ratio of the axial velocity near the tube wall is 4.

The existence of two types of vortex symmetry means that the set of integral flow parameters Equation 6 is, in general, insufficient for classification of swirling pipe flows. As a consequence, flows with the same Reynolds number (1) and the same swirl number (2), but with different helical symmetry of the vorticity field will differ from the mass transfer point of view. This effect will be analysed quantitatively in the next paragraphs.

4. Mass flux to the wall in the boundary layer of swirl flow

Here we calculate Sherwood number as a function of the inviscid swirl flow parameters. The traditional methodology for hydrodynamic and diffusion boundary layers will be used without any empirical hypotheses or 'analogy' arguments. For large Schmidt numbers, the diffusion layer lies within a thin region of the hydrodynamic boundary layer. For this reason, it is possible to neglect the curvature of the tube and to use a planar coordinate system which is related to the wall, see Figure 7.

We first calculate the velocity profile in the hydrodynamic boundary layer of the axisymmetric swirl flow in the tube. The presence of the two velocity components in the inviscid flow core leads to the 3D equations for hydrodynamic boundary layer:

$$\begin{cases} u_y \dfrac{\partial u_x}{\partial y} + u_z \dfrac{\partial u_x}{\partial z} = \nu \dfrac{\partial^2 u_x}{\partial y^2} \\ u_y \dfrac{\partial u_z}{\partial y} + u_z \dfrac{\partial u_z}{\partial z} = \nu \dfrac{\partial^2 u_z}{\partial y^2} - \dfrac{1}{\rho}\dfrac{\partial p}{\partial z} \\ \dfrac{\partial u_y}{\partial y} + \dfrac{\partial u_z}{\partial z} = 0 \end{cases} \tag{8}$$

with the following boundary conditions:

$$y = 0 : u_x = u_y = u_z = 0$$

and

$$y = \infty : \quad u_x = w_\varphi(R) \equiv V; \quad u_z = w_z(R) \equiv W$$

The assumption that the flow is axisymmetrical is taken into account in Equation 8, so all flow characteristics invariant in the tangential direction (x axis). Equation 8 are exactly the same as those obtained in [23] for the case of axisymmetrical flow along a body.

For further simplifications of Equation 8, it may be noted that $\partial p/\partial z = 0$. Indeed, we assume that friction losses do not influence the inviscid flow core over the entire mass transfer section (this means constancy of the velocities V and W). So, the pressure term in the second equation of (8) vanishes, and the first equation of the

Table 1. Comparisons of intensity of mass transfer in swirl flows with different parameters

Type of vortex	Regime parameters			Vortex parameters				Velocities near wall		$\overline{Sh}_{swirl}/\overline{Sh}_{axial}$	
	Re	S_d	S	Γ/UR^2	$2\pi\, l/R$	a/R	w_0/U	W/U	V/U	(section)	(electrode)
Set-up with tangential vane swirler [20]											
Right-handed	11480	0.79	0.32	2.1	1.9	0.24	1.9	0.9	0.34	0.98	0.97
Left-handed	11480	0.79	0.30	2.0	−2.6	0.38	0.38	1.1	0.32	1.03	1.06
Set-up with axial-tangential input [21]											
Axial flow	2.8×10^5	0.0	0.0	–	–	–	1.0	1.0	0.0	1	1
Right-handed	2.8×10^5	0.1	0.09	1.2	7.2	1.0	1.08	0.91	0.19	0.95	0.96
Right-handed	2.8×10^5	0.35	0.32	2.6	14	0.65	1.15	0.97	0.41	0.98	1.01
Left-handed	2.8×10^5	0.7	0.6	4.4	−6.7	0.5	0.47	1.12	0.70	1.06	1.12
Set-up with rotating honeycomb section as swirler [22]											
Right-handed	2.8×10^5	0.5	0.32	3.7	10.8	0.9	1.12	0.85	0.58	0.92	0.98
Right-handed	2.8×10^5	1.0	0.6	7.1	14.8	0.9	1.27	0.79	1.13	0.88	1.07
Model vortices under the same flow parameters: G, Q, M, J, E											
Right-handed	inviscid flow and imaginary swirler		1.96	2.667	1.64	0.42	2.4	0.86	2.667	0.93	1.37
Left-handed			0.95	2.667	−0.667	1.0	−0.98	3.0	2.667	1.73	1.91

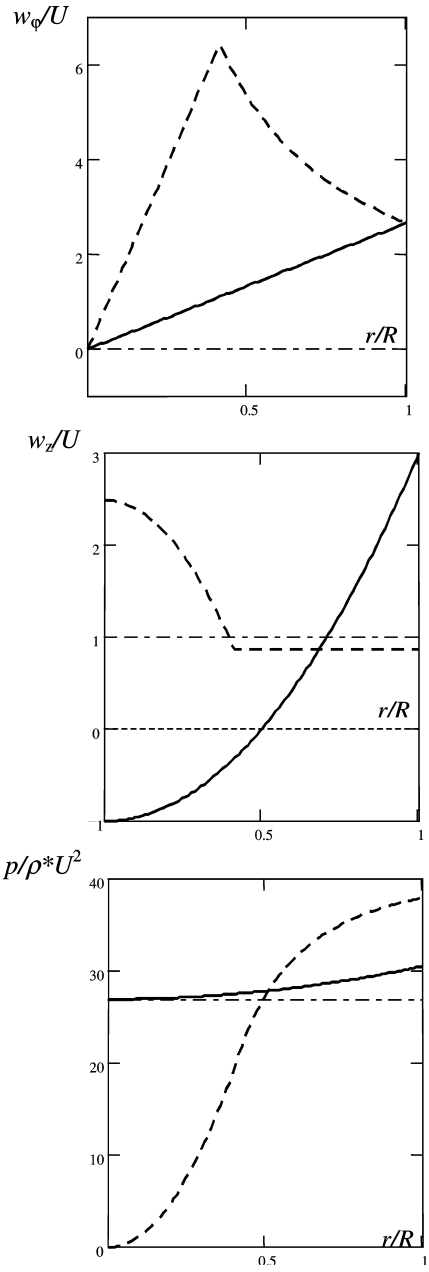

Fig. 6. Tangential (w_φ), axial (w_z) velocities and pressure distribution (p) for model swirl flow, results of numerical simulations (3D effects are neglected): (*dashed line*) right handed helical vortex; (*solid line*) left handed helical vortex.

system (8) becomes identical with the second. Thus, the two velocity components become proportional, exactly as in the case of axisymmetrical flow along a body [23]:

$$\frac{u_x}{u_z} = \frac{u_\varphi}{u_z} = \frac{V}{W} \tag{9}$$

Moreover, the second and the third equations of the system (8) become identical with the equations for a boundary layer on a flat plate. So, the solution of the system (8) may be presented in the form:

$$\begin{cases} u_\varphi = u_x = V\phi' \\ -u_r = u_y = \frac{1}{2}\sqrt{\frac{\nu W}{z}}(\xi\phi' - \phi) \\ u_z = W\phi' \end{cases} \tag{10}$$

Here, the function ϕ is a solution of the Blasius equation [23]. Thus, the local shear stress at the tube wall is given by the equations:

$$\tau_z = \mu\frac{\partial u_z}{\partial y}\bigg|_{y=0} = 0.332\sqrt{\frac{\mu\rho W}{z}}W \tag{11a}$$

and

$$\tau_\varphi = \mu\frac{\partial u_x}{\partial y}\bigg|_{y=0} = 0.332\sqrt{\frac{\mu\rho W}{z}}V \tag{11b}$$

where μ is the dynamic viscosity and ρ is the fluid density.

To describe of mass transfer in the hydrodynamic boundary layer, we use the steady convective diffusion equation [18], which in cylindrical coordinates takes the form:

$$u_r\frac{\partial c}{\partial r} + u_\varphi\frac{\partial c}{r\partial\varphi} + u_z\frac{\partial c}{\partial z} = D\left(\frac{\partial}{r\partial r}\left(r\frac{\partial c}{\partial r}\right) + \frac{\partial^2 c}{r^2\partial\varphi^2} + \frac{\partial^2 c}{\partial z^2}\right) \tag{12}$$

In the diffusion layer, we may use the usual expansion for the velocity components (u_r, u_φ, u_z), with respect to the distance from the wall $y = R - r$:

$$u_z = (r-R)\frac{\partial u_z}{\partial r}\bigg|_{r=R} \quad \text{and} \quad u_\varphi = (r-R)\frac{\partial u_\varphi}{\partial r}\bigg|_{r=R}$$

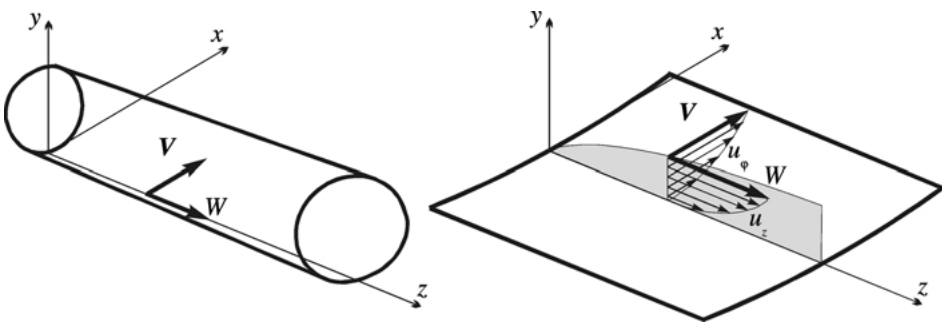

Fig. 7. System of coordinates for three-dimensional boundary layer in a tube.

$$u_r = \left[\frac{1}{2}(r-R)^2\frac{\partial^2 u_r}{\partial r^2}\right] = -\frac{1}{2}(r-R)^2\left(\frac{1}{R}\frac{\partial}{\partial\varphi}\frac{\partial u_\varphi}{\partial r}+\frac{\partial}{\partial z}\frac{\partial u_z}{\partial r}\right)\Bigg|_{r=R} \quad (13)$$

In Equation 13 the last relation for the radial component of the velocity (u_r) is a consequence of the continuity equation.

As the curvature of the diffusion layer is small with respect to tube radius, we replace the cylindrical problem by the planar one. The additional simplification of Equation 12 follows from the boundary layer approximation (longitudinal and transversal molecular diffusion are neglected). As a result, Equation 12 takes the form:

$$\frac{\tau_z}{\mu}y\frac{\partial c}{\partial z}-\frac{1}{2\mu}\frac{\partial\tau_z}{\partial z}y^2\frac{\partial c}{\partial y}+\frac{\tau_\varphi}{\mu}y\frac{\partial c}{\partial x}=D\frac{\partial^2 c}{\partial y^2} \quad (14)$$

where the shear stress τ at the tube wall is given by Equation 11.

The boundary conditions for Equation 14 depend on the concentration boundary conditions. Two cases are of importance: (i) mass transfer (global or local) over a section of the tube [1,5], and (ii) mass transfer at the surface of a microelectrode flush mounted with the tube wall [7]. We first consider the problem when the mass transfer section is a part of a tube of length L. In this case, the boundary conditions for Equation 14 are:

$$\begin{aligned} &c = c_\infty \text{ for } z = 0 \text{ or } y \to \infty \\ &c = 0 \text{ for } y = 0 \text{ and } 0 \le z \le L \end{aligned} \quad (15)$$

As the boundary conditions (Equation 15) do not depend on the tangential coordinate x, we can neglect this dependence in Equation 14. Thus, the convective mass transfer in the tangential direction may be omitted and the integration of Equation 14 with the boundary conditions of Equation 15 can be done exactly as for the diffusion to a flat plate [18]. As a result, the following expression for the mass transfer coefficient to the tube wall is obtained:

$$k(z) = -\frac{D}{c_\infty}\frac{\partial c}{\partial y}\Bigg|_{y=0} = \frac{D}{\delta(z)} \quad (16a)$$

$$\delta(z) = 2.95\,Sc^{-1/3}\left(\frac{vz}{W}\right)^{1/2} \quad (16b)$$

Accordingly, the average Sherwood number is given by:

$$\overline{Sh} = \frac{1}{D}\int_0^L k(z)\,dz = 0.678\,Sc^{1/3}\left(\frac{WL}{v}\right)^{1/2} \quad (17)$$

Within the frame of the model (e.g., by neglecting turbulent and 3D effects), the regular inviscid swirl flow (with W = cte, V = cte) generates hydrodynamic and diffusion boundary layers similar those developing on a flat plate, since:

$$\delta(z) \sim \sqrt{z}$$

Equations 16 and 17 can be used for the prediction of mass transfer in relatively short mass transfer sections, when the influence of friction losses on inviscid flow core is negligible.

In the case of mass transfer on the surface of a circular microelectrode flush mounted with the wall, the mass flux to a surface is defined by the modulus of the local shear stress and depends on both the axial and the tangential velocity components of the inviscid flow core. If the microelectrode is far enough from the flow input, it is possible to neglect the variations of local shear stress along the electrode surface and to reduce the problem to the Leveque solution [24]. Therefore, the following expression is obtained for the average microelectrode Sherwood number:

$$\overline{Sh} = 0.866\left(\frac{\sqrt{\tau_z^2+\tau_\varphi^2}\big|_{z=z_0}\,d_0^2}{\mu D}\right)^{1/3} \quad (18)$$

Here, d_0 is the microelectrode diameter and z_0 is its longitudinal coordinate. Substituting the expression for the local shear stress Equation 11 into Equation 18, we obtain:

$$\overline{Sh} = 0.6\,Sc^{1/3}\left(\frac{d_0}{z_0}\right)^{1/6}\left(\frac{d_0\left(W(V^2+W^2)\right)^{1/3}}{v}\right)^{1/2} \quad (19)$$

5. Mass transfer in swirl flows with a different helical symmetry of vorticity field

In this Section, we shall analyse the influence of different types of helical symmetry on mass transfer. The traditional approach to mass transfer in swirl flows is based on Equation 3, where Re is the main parameter and the empirical constant α and the power n depend on the swirl number S. In Section 3, we have demonstrated that under the same flow conditions (Re, S constant) two different types of swirl flow may exist with jet- and wake-like profiles of axial velocity. These two flow regimes were observed [11, 12 and 25] in swirl flows with vortex breakdown with a wide range of Reynolds number (from 1500 to 300 000). Thus, the traditional correlation of Sherwood number by means of Equation 3 is, in general, insufficient.

To quantitatively examine this problem, we have used experimental data of [20–22] and the above-mentioned numerical simulations of velocity profiles (Figures 2–4 and 6). In order to simplify comparison of mass transfer in different swirl flows, all the results are presented in

Table 1. Three different experimental set-ups and one virtual swirl flow obtained by means of numerical simulation are given in this Table. The first three columns of Table 1 give some hydrodynamic parameters traditional for swirl flows—the Reynolds number Re and the swirl number S. For the swirl number, we use the definition given by the authors (S_d), which is specific for each set-up, and the more general definition by means of the Equation 2. Columns 4–9 give the parameters of the inviscid flow core, which were obtained by means of Equations 4 and 5 and experimental information reported in [20–22]. Column 4 gives the flow circulation (Γ); columns 5 and 6 give the pitch of vortex lines (l) and the radius of the vortex core (ε) (Figure 1 and Equations 4 and 5); columns 7–9 give the axial component of the inviscid flow on the axis (w_0) and near the wall (W) and the tangential component of the inviscid flow near the wall (V). In the last two columns we give the ratio of Sherwood number for swirl flow to the Sherwood number for axial developing flow with the same flow rate. Column 10 corresponds to the case where the mass transfer section is part of tube wall, Equation 17. Finally column 11 correspond to the case of mass transfer on the surface of a microelectrode, Equation 19.

We first consider the flow with vortex breakdown (Figure 2), generated by a tangential vane swirler [20]. For this flow, we can predict the difference in mass transfer characteristics for different types of vortices. This difference is not very pronounced because of the small value of the swirl number S. One can see that left-handed vortex increases the mass transfer in comparison to axial developing flow with the same Re number. The right-handed vortex is not so efficient and can even decrease the mass transfer with respect to the axial developing flow.

A similar conclusion can be obtained from the analysis of flow regimes obtained on two other experimental set-ups with a cylindrical working section. In the first set-up [21] the swirl flows were induced by an axial–tangential inlet. In the second set-up [22] a rotating honeycomb section was used as the swirler. It is possible to see a lack of similarity between the flows with the same Re for the case where the swirl number $S = 0.6$. Indeed, the transition from a jet-like to a wake-like axial velocity profile was observed with increase of the swirl number from 0.32 up to 0.6 in [21], whereas this effect was not noted in [22]. A comparison of mass transfer in these flows for both set-ups gives a rather pronounced (about 20%) difference in Sherwood number for flows with the same values of Re and S, but with different helical symmetry of the vorticity field.

The difference in mass transfer related to the vortex symmetry can be essential, as shown by the example of a model vortex (last two lines in Table 1). We have simulated two velocity profiles of inviscid flow Equation 5 which have the same integral flow parameters (Equation 6), but different type of helical symmetry of the vorticity field. Conservation of all integral flow parameters (Equation 6) is essential for correct comparison of different flow regimes. For this case, the left-handed vortex is about two times more efficient with respect to mass transfer than the right handed vortex. The right-handed vortex decreases the mass transfer in comparison to the developing axial flow with the same Re.

6. Discussion and conclusions

The mathematical model of mass transfer in swirl flows developed in this work can be used for both academic and engineering purposes. Traditional notions of 'continuous' and 'decaying' swirl flows should be specified. In this study we have used a model of a regular (or established) inviscid vortex core. The established vortex core can exist over relatively short mass transfer sections where the influence of friction losses is not important. For this type of swirl flow, for an experimenter providing LDA measurements in the inviscid core, the regime is 'established'. On the other hand, the local shear stress and local mass transfer coefficient in this flow vary along the mass transfer section, as well as on the flat plate. So, for an experimenter providing electrochemical flow measurements by means of flush mounted microelectrodes the flow is 'decaying'. Clearly, the development of an inviscid vortex core along the mass transfer section is also possible due to friction losses or/and 3D and turbulent effects. The study of these effects is not the object of this paper.

Secondly, the model gives an explanation of the effect the duality of swirl motion on mass transfer. Usually, it is reported that swirl flows increase mass transfer in comparison with axial flows at the same Re. Nevertheless, there are experimental data showing that swirl can decrease mass transfer, especially for low Re. For example, in [2] it is reported that, in the entrance region of decaying annular swirl flow, mass transfer is smaller than in axial flow for $Re < 6000$. The data reported in [5] also indicate some regimes ($Re = 3348$) where the local mass transfer in annular swirl flow decreases with respect to fully developed annular flow. The data of [3] show that, depending from the position of the mass transfer section with respect to the flow inlet, the mass transfer coefficient in pure swirl flow for the laminar regime ($Re < 1000$) can be larger or smaller than that in developing laminar axial flow in annulus. This duality can be explained by the existence of two types of axisymmetrical swirl flow. Swirl flows with wake-like velocity profile increase the mass transfer, whereas swirl flows with jet-like velocity profile are not so efficient, and can even decrease mass transfer in comparison to axial flows. 3D effects in mass transfer, which are not taken into account in the present study, can compensate the relative decrease of mass transfer due to the jet-like character of the axial velocity.

It is also important to emphasize that the model shows that, in swirl flow, the correlations of Sherwood

number by means of two hydrodynamic parameters (the Reynolds and the swirl numbers) are, in general, insufficient. Indeed, in swirl flow with the same integral characteristics two types of vortex structures can exist, with left-handed and right-handed helical symmetry. The left-handed helical vortexes generate wake-like swirl flows and the right-handed vortex structures generate jet-like swirl flows. Our estimations show (Table 1) that under the same integral flow characteristics the change in vortex symmetry can increase the mass transfer by a factor of at least two.

From the engineering point of view, this study leads to two important conclusions: (i) in swirl devices it is preferable to generate left-handed vortex structures in order to increase mass transfer; and (ii) spontaneous transition from on to another type of vortex symmetry is possible in swirl devices even if all the integral flow parameters are well controlled. The transition to another vortex symmetry can provoke a significant change in mass transfer characteristics (by at least a factor of two).

Acknowledgement

This work was carried out in the laboratory LET UMR CNRS no. 6608. The authors warmly thank the University of Poitiers and the Ministry MESRT of France, for making this work possible by granting a position as visiting professor to one of them.

References

1. P. Legentilhomme and J. Legrand, *Int. J. Heat Mass Transf.* **34** (1991) 1281.
2. M.S. de Sa, E. Shemilt and I.V. Soegiarto, *Can. J. Chem. Eng.* **69** (1991) 294.
3. P. Legentilhomme, A. Aouabed and J. Legrand, *Chem. Eng. J.* **52** (1993) 137.
4. S. Yapici, M.A. Patrick and A.A.Wragg, *Int. Com. Heat Mass Transf.* **21** (1994) 41.
5. S. Yapici, M.A. Patrick and A.A. Wragg, *J. Appl. Electrochem.* **24** (1994) 685.
6. S. Yapici, M.A. Patrick and A.A. Wragg, *J. Appl. Electrochem.* **25** (1995) 15.
7. S. Yapici, G. Yazici, C. Ozmetin, H. Ersahan and O. Comakli, *Int. J. Heat Mass Transf.* **40** (1997) 2775.
8. G. Lefèbvre, S.R. Farias Neto, H. Aouabed, P. Legentilhomme and J. Legrand, *Can. J. Chem. Eng.* **76** (1998) 1039.
9. M.N. Noui-Mehidi, A. Salem, P. Legentilhomme and J. Legrand, *J. Appl. Electrochem.* **29** (1999) 1277.
10. S.V. Alekseenko, P.A. Kuibin, V.L. Okulov and S.I. Shtork, *J. Fluid Mech.* **382** (1999) 195.
11. S. Leibovich, *Ann. Rev. Fluid Mech.* **10** (1978) 221.
12. M. Escudier, *Prog. Aerosp. Sci.* **25** (1988) 189.
13. A. Gupta, D.G. Lilley and N. Syred, 'Swirl flow', (Abacus Press, Cambridge, 1984).
14. V.L. Okulov, *Tech. Phys. Lett.* **22** (1996) 798.
15. V. Okulov, S. Alekseenko, J. Legrand and P. Legentilhomme, *Russ. J. Eng. Thermophys.* **7** (1997) 149.
16. T. Murakhtina and V. Okulov, *Tech. Phys. Lett.* **26** (2000) 432.
17. T. Murakhtina and V. Okulov, Modelling of the turbulent vortex breakdown as a transition from column to conical helical vortices, *in* S. Dopazo (Ed.), 'Advance in Turbulence', Vol. 8 (Barcelona, 2000), pp. 817–820.
18. V.A. Levich, 'Physicochemical Hydrodynamics' (Prentice Hall, Englewood Cliffs, NJ, 1962).
19. P.A. Kuibin and V.L. Okulov, *Thermophys. & Aeromech.* **3** (1996) 335.
20. A.K. Garg and S. Leibovich, *Phys. Fluids* **22** (1979) 2053.
21. O.G. Dahlhaug, 'Thesis Doctor Engineer', NTNU, Trondheim, Norway (1997).
22. M. Schmidts and V. Vasanta, Ram Turbulence characteristics in pipe flow with swirl, *in* S. Dopazo (Ed.), 'Advances in Turbulence', Vol. 8 (Barcelona, 2000) pp. 121–124.
23. H. Schlichting, 'Boundary-Layer Theory', (McGraw-Hill, 7th edn, New York, 1979).
24. J. Leveque, *Ann. Mines* **13** (1928) 201.
25. T. Sarpkaya and F. Novak, *AIAA Paper* 99–0135 (1999).